Isoreticular two-dimensional magnetic coordination polymers prepared through pre-synthetic ligand functionalization

J. López-Cabrelles[1$], S. Mañas-Valero[1$], I. J. Vitórica-Yrezábal[2], P. J. Bereciartua[3+], J. A. Rodríguez-Velamazán[4], J. C. Waerenborgh[5], B. J. C. Vieira[5], D. Davidovikj,[6] P. G. Steeneken,[6] H. S. J. van der Zant,[6] G. Mínguez Espallargas[1]* and E. Coronado[1]*.

[$] These authors contributed equally to this work.

[1] *Instituto de Ciencia Molecular (ICMol), Universitat de València, c/Catedrático José Beltrán, 2, 46980 Paterna, Spain.*

[2] *School of Chemistry, University of Manchester, Oxford Road, Manchester, M13 9PL, UK.*

[3] *Instituto de Tecnología Química (UPV-CSIC), Universitat Politècnica de València−Consejo Superior de Investigaciones Av. de los Naranjos s/n, 46022 Valencia, Spain.*

[4] *Institut Laue-Langevin, 71 Avenue des Martyrs, CS 20156, 38042 Grenoble Cedex 9, France.*

[5] *Centro de Ciências e Tecnologias Nucleares, Instituto Superior Técnico, Universidade de Lisboa, 2695-066 Bobadela LRS, Portugal.*

[6] *Kavli Institute of Nanoscience, Delft University of Technology, Lorentzweg 1, Delft 2628 CJ, The Netherlands.*

[+] *Current address: Deutsches Elektronen-Synchrotron (DESY), Notkestraße 85, 22607 Hamburg, Germany.*

Chemical functionalization is a powerful approach to tailor the physical and chemical properties of two-dimensional materials, increase their processability and stability, tune their functionalities and, even, create new 2D materials. This is typically achieved through post-synthetic functionalization by anchoring molecules on the surface of an exfoliated 2D crystal, but it inevitably alters the long-range structural order of the material. Here we present a pre-synthetic approach that allows the isolation of crystalline, robust, and magnetic functionalized monolayers of coordination polymers. A series of five isoreticular layered magnetic coordination polymers based on Fe(II) centres and different benzimidazole derivatives (bearing a Cl, H, CH_3, Br or NH_2 side group) were first prepared. On mechanical exfoliation, 2D materials are obtained that retain their long-range structural order and exhibit good mechanical and magnetic properties. This combination, together with the possibility to functionalize their surface at will, makes them good candidates to explore magnetism in the 2D limit and to fabricate mechanical resonators for selective gas sensing.

Since the isolation of graphene, there has been an explosion in the search for other atomically thin layers (aka. 2D materials).[1] Most of these graphenoid compounds are layered inorganic materials that in bulk show stacked structures with weak van der Waals interactions between adjacent sheets, but with strong covalent bonding within each sheet. These materials cover a wide range of physical properties including insulators (h-BN),[2] semiconductors (1T-ZrS_2, 2H-MoS_2 or black phosphorous),[3–5] metals (1T-MoS_2),[6] and superconductors (Mo_2C, 2H-$NbSe_2$ or 2H-TaS_2).[7–9] However, 2D magnetic materials (V_5S_8, $FePS_3$, $Cr_2Ge_2Te_3$ or CrI_3)[10–13] have remained elusive until recently, due to their unstability at ambient conditions and the difficulty to experimentally detect magnetism in the 2D limit. In fact, this challenging issue has only been achieved so far in the most favorable case (Ising ferromagnet).[13]

Recently, a new and less explored field has emerged with 2D organic polymers (including covalent organic frameworks, COFs, and conjugated aromatic polymers, CAPs),[14,15] and 2D coordination polymers (enclosing coordination polymers, CPs, and metal-organic frameworks, MOFs),[16] which have been employed for membranes[17], gas separation[18], electronics[19] and photoluminescence.[20] However, due to the fragility of the starting crystals, there are only a few examples that can be exfoliated micromechanically, although with limited lateral dimensions,[15,21] being liquid exfoliation the most common methodology.[17,22] This prevents application of these exfoliated materials in areas where high-quality layers are required (nanoelectronics, for example), the most recent uses being in the fields of catalyisis[23] and membranes.[24]

A crescent interest in the field of 2D materials resides in their covalent functionalization, since surface engineering can lead to the rational modification of surface properties (hydrophobicity, adhesivity or wettability, among others), or electronic properties of the layers.[25,26] As the surface modifications are generally performed following a post-synthetic method, high rates of surface functionalization are often challenging due to the poor reactivity and solubility of the inorganic surfaces.[27] Therefore, the molecules are anchored to the surface in a random way leading to a defective and incomplete functionalization of the layered material. An alternative strategy for the chemical surface modification is the pre-synthetic method

where the bulk layered material is chemically modified prior to the exfoliation. This approach, unfeasible in 2D inorganic materials, can be easily achieved in 2D coordination polymers due to the molecular composition of these compounds. Thus, through the rational choice of the functional substituent of the organic ligand, it is possible to achieve a periodically ordered decoration of the 2D coordination network, i.e. a defect-free functionalized 2D material (Figure 1).

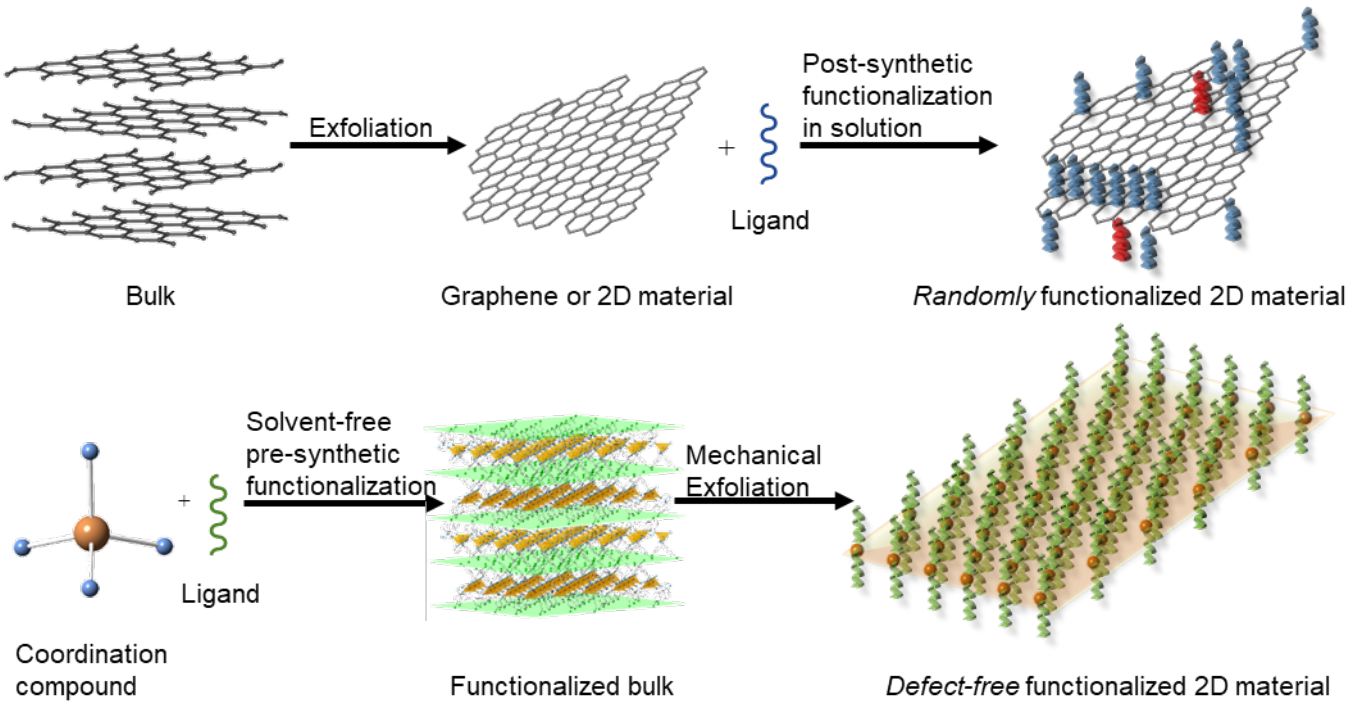

Figure 1 | Schematic representation of the post-synthetic covalent functionalization vs. the pre-synthetic functionalization used here. The top part exemplifies the commonly used strategy to functionalize two-dimensional (inorganic) materials consisting on two steps: i) mechanical or liquid exfoliation of the bulk material; ii) functionalization in solution of the exfoliated material, yielding a random distribution of the functional groups, represented in blue. This route can also produce ligand modifications, represented with a colour change from blue to red. The bottom part indicates a pre-synthetic functionalization in which the functionalized bulk is first obtained prior to be mechanically exfoliated, thus yielding a quasi-perfect array of unaltered functional groups attached to the surface.

Here we present a new family of layered coordination polymers (LCPs), **MUV-1-X** (MUV = Material of the University of Valencia), of general formula $[Fe(bimX)_2]$ (HbimX = derivative of benzimidazole, with X = H, Cl, Br, CH_3, or NH_2) which exhibit cooperative magnetism and which are robust enough to be micromechanically exfoliated down to the monolayer, while preserving their crystallinity. The pre-synthetic modification of the materials through the convenient choice of the organic substituent gives rise to a surface tunability ranging from hydrophilic to hydrophobic, albeit maintaining the inner physical property (i.e. magnetic order) in all the derivatives of the family.

Results

Synthesis and characterization of the layered coordination polymers

The solvent-free reaction of 5-chlorobenzimidazole (HbimCl) and ferrocene, adapting a previously described method for the preparation of iron azolates,[28] yields large laminar colorless crystals of formula $[Fe(bimCl)_2]$ (abbreviated as **MUV-1-Cl**), consisting of distorted tetrahedral Fe^{II} centers connected by 5-chlorobenzimidazolate bridges (Figures 2a and 2b) forming a neutral layered coordination polymer extended in the *ab* plane. These layers weakly interact with each other through van der Waals interactions (Cl···Cl interactions). The compound is related to the diamagnetic Zn analogue $[Zn(bimH)_2]$, which was obtained via decomposition of a 3D MOF.[17] In these atomically thin layers, the Fe^{II} atoms are located in the inner part of the layers whereas the Cl substituents are positioned at the surface (Figure 2a), thus playing an active role in the chemical behavior of the molecular interface. A close-up view with scanning electron microscopy (SEM) evidences the layered structure of **MUV-1-Cl** as the stacking of multiple sheets (Figure 2c), with a typical size of 400 μm approximately, whose purity is confirmed by powder X-ray diffraction (Supplementary Fig. 8). The room temperature infrared and Raman spectra present coincident peaks, indicating a non-centrosymmetric structure (Supplementary Fig. 40). Furthermore, room temperature Mossbauer spectra consist of two doublets with the same relative area for Fe^{II}, indicating the presence of two different Fe^{II} sites with the same multiplicity (Supplementary Fig. 12).

These features are consistent with the space group *C*2, although the presence of a racemic mixture causes a better refinement of the single crystal X-ray data in the *C*2/*c* space group. This is related to the weak interlayer interactions, which prevent long range order in the *c* direction, but which is advantageous for exfoliation.

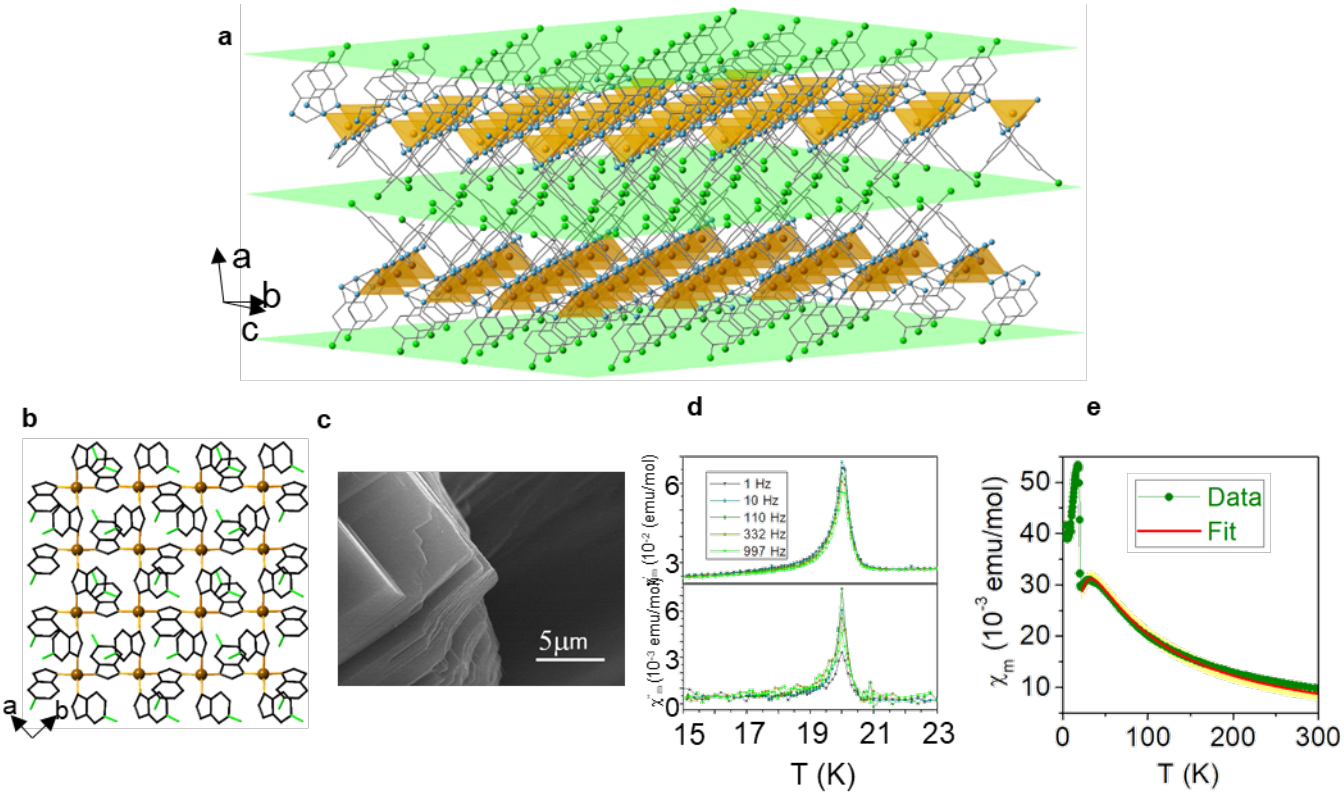

Figure 2 | Bulk characterization of MUV-1-Cl. a, Layered structure of **MUV-1-Cl** showing the Cl atoms located at the surface of the layers, represented as green planes. Iron centers shown in orange (polyhedral representation), nitrogen atoms shown in blue, carbon atoms shown in black and chlorine atoms shown in green. Hydrogen atoms have been omitted for clarity; **b**, Structure of a single layer of **MUV-1-Cl** viewed along the *c* axis (i.e. *ab* plane). Same color code as in panel a; **c**, Scanning Electron Micrograph of the bulk material, clearly showing the layered structure; **d**, Temperature dependence of the in-phase (top) and out-of-phase (bottom) dynamic susceptibility of **MUV-1-Cl** measured at different frequencies; **e**, Thermal dependence of the magnetic susceptibility in the temperature range 2-300 K. The data have been fitted following a Lines expansion for a quadratic-layer Heisenberg antiferromagnet with S = 2 [29]. The yellow line represents the prediction bands with a confidence interval of 95%.

The short pathway between the iron centers, provided by the 5-chlorobenzimidazolate bridges, facilitates the presence of magnetic exchange in **MUV-1-Cl**, as evidenced in the plot of the molar magnetic susceptibility (χ_m) as a function of the temperature (Fig. 2d and Supplementary Section 5.2). The χ_m *vs.* T curve exhibits a broad maximum at 30.0 K and a sharp peak at *ca.* 20 K. In the plot of $\chi_m T$ *vs.* T, a $\chi_m T$ value of 2.94 emu·mol^{-1}·K is observed at room temperature, in agreement with that expected for a high-spin Fe^{II}, S = 2 (3.0 emu·mol^{-1}·K where g = 2.0), which decreases upon cooling down to 20 K (Supplementary Fig. 17). The behavior in this region indicates the presence of dominant antiferromagnetic (AF) exchange coupling between the Fe^{II} centres, confirmed by a negative Curie-Weiss temperature, θ = –80.6 K (Supplementary Fig. 16). These data can be quantitatively reproduced using a model for a quadratic-layer Heisenberg antiferromagnet[29] with S = 2 ($H = -\sum_{i,j} JS_i \cdot S_j$) (Figure 2d and Supplementary Fig. 15). The resulting exchange parameter is J = –22.9 cm^{-1}. The abrupt increase in both χ_m and $\chi_m T$ suggests the occurrence of a magnetic transition towards a canted spin structure below the Néel temperature, T_N, of 20 K. The presence of an out-of-phase susceptibility signal below 20 K in the *ac* measurements confirms this kind of magnetic order (Figure 2e and Supplementary Fig. 18). Powder neutron diffraction patterns collected at 1.8 K and 30 K, i.e. below and above the ordering temperature (Supplementary Section 5.1), provide a further support on the antiferromagnetic ordering in this material. Still, in the present case these measurements are unable to detect the presence of spin canting, which is below the limit of detection of these measurements (Supplementary Section 5.1), mainly due to the small value of the ferromagnetic component resulting from canting as deduced from susceptibility measurements.

From bulk crystals to the 2D limit

The layered nature of **MUV-1-Cl** and the absence of strong intermolecular interactions between adjacent layers prompted us to explore the possibility of mechanically exfoliating this material by the so-called *Scotch-tape method*, a conventional approach usually employed for graphene and other two-dimensional materials, but rather scarce in coordination polymers due to the fragile nature of the

crystals.[21] The advantage of this dry method over liquid exfoliation is the potential achieving of atomically thin-layers with high crystallinity and larger lateral sizes.

Bulk crystals of **MUV-1-Cl** were exfoliated using a plastic tape (Ultron Systems) and deposited onto a silicon substrate with 285 nm of thermally grown SiO_2. As a result, a plethora of flakes with remarkable well-defined rectangular shapes (lateral dimensions > 1 μm) and different thicknesses (ranging from a single layer up to hundreds of nanometers) were obtained, as can be clearly seen by optical and atomic force (AFM) microscopies (Supplementary Fig. 22-28), thus being air-stable. This contrasts with the lower quality nanosheets obtained in a Zn analogue compound by liquid exfoliation.[17] Remarkably, a monolayer of dimensions 4 x 1.5 μm^2 has been isolated (Figure 3a and Supplementary Section 6.2). The crystallinity, chemical composition and integrity of the exfoliated flakes was confirmed through Transmission Electron Microscopy (TEM) and Raman studies on specimens of different thicknesses (Figures 3b and 3d and Supplementary Section 6). To the best of our knowledge, this is the first time that selected-area electron diffraction (SAED) patterns have been obtained in a top-down micromechanically exfoliated LCP (Figure 3d), and previously this has only been achieved with inorganic materials, mainly members of transition metal dichalcogenides.[30,31] There are some features that could be associated to diffuse scattering, resulting from the presence of a modulated commensurate structure in the bulk material (see Supporting Information Sections 2 and 6.4). The indexation of these patterns indicates that they correspond to the zone axis [0 0 1], confirming that the exfoliated flakes consist of one or several layers whose stacking along the *c* axis forms the original bulk material. The close resemblance between the experimental and the simulated patterns (Figure 3d and Supplementary Section 6.4) provides further evidence of that. Moreover, the well-defined Bragg peaks observed in the SAED patterns point out that the exfoliation process does not damage the structure of the LCP, and the obtained flakes retain the crystallinity of the bulk material. Note that some of the SAED patterns were obtained from layers as thin as 20 nm, that is a remarkable result due to the molecular nature of the material. It was not observed any thickness-dependence of the unit cell or Raman peaks shift, compared to their bulk counterparts.

The magnetic order of the atomically thin-layers deposited in a silicon substrate was inspected by Magnetic Force Microscopy at Low-Temperatures (LT-MFM) in a dual-pass mode configured with a phase locked loop (PLL) feedback on the cantilever oscillation (Supplementary Section 6.5). In this configuration, the magnetic signal is related to the frequency shift (Δf) in such a way that an attractive tip-sample interaction is characterized by $\Delta f < 0$ (red contrast) and a repulsive tip-sample interaction is characterized by $\Delta f > 0$ (blue contrast).[32] For simplicity in the comparison of the magnetic images, we have defined in this work the frequency shift to be 0 (green contrast) in the silicon substrate.[33] Below the order temperature, the flakes are imaged with a smoothly red contrast, indicative of an attractive tip-sample interaction, that disappears at temperatures above T_N (Figure 3c), in agreement with a transition from a canted AF structure to a paramagnetic phase. In addition, as expected from the magnetic structure of the material (weak ferromagnet due to an antiferromagnetic canted structure), this contrast is very weak and furthermore it remains unaffected by the reversal of an applied in-plane external field (from +2 T to –2 T). Hence, from these measurements we cannot conclude that the signal has a pure magnetic component as it may be also influenced by other forces as the electrostatic ones. Low-temperature nano-MOKE measurements and Kelvin-probe microscopy on individual sheets will be performed in the future to get further information on this issue.

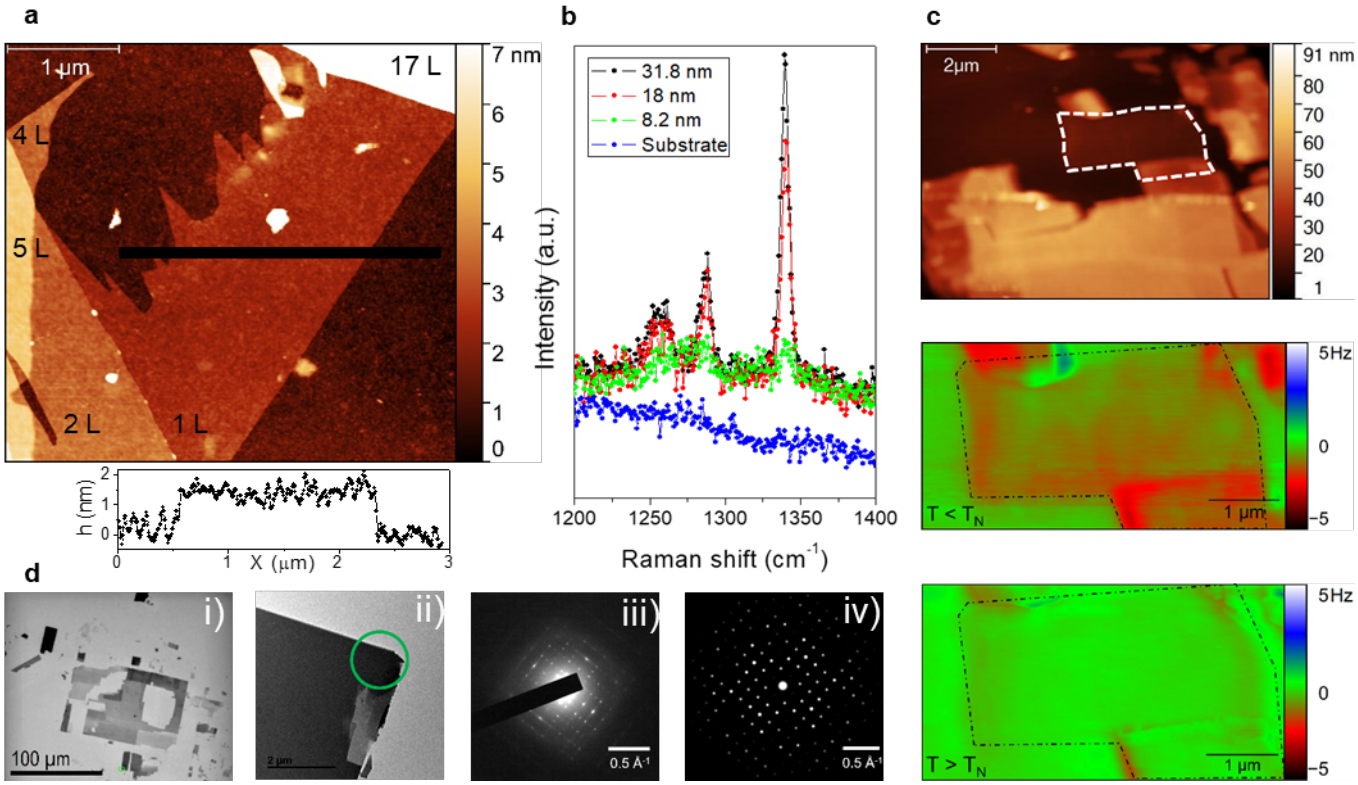

Figure 3 | Atomically thin layers of MUV-1-Cl. a, Atomic-force image with its profile of height for a flake of **MUV-1-Cl** (see Supporting Section 6.2 for further information). Different number of exfoliated layers are indicated in the image; **b**, Raman spectra for **MUV-1-Cl** flakes with different thicknesses; **c**, MFM measurements of a 5.7 nm thick flake of **MUV-1-Cl**. (top) general topography image of the selected region with the flake highlighted in dashed white line; (middle and bottom) MFM images of the flake highlighted in dotted black line showing the difference in frequency shift below (middle panel) and above T_N (bottom panel). Note the change in colour contrast below T_N, which indicates an attractive tip-sample interaction in the ordered state, that disappears at temperatures above T_N. See Supplementary Section 6.5 for further information; **d**, I, Low-magnification TEM image for **MUV-1-Cl** flakes, where darker gray areas are associated to thicker flakes. ii-iv, A selected area (enclosed by a green circle on the TEM image in ii) for which the experimental SAED pattern was obtained that corresponds to the [0 0 1] zone axis (iii), and which is in very good agreement with the simulated SAED pattern (iv).

Surface modification

Surface engineering is a demanding challenge in 2D materials since it permits to tune the surface chemistry at will (modifying, for example, the hydrophobicity/hydrophilicity) and, subsequently, opens the door for the use of these systems in an industrial and technological relevant scale. However, many of the reported processes to modify the surface of 2D materials lead to defective materials that change their electronic or magnetic properties[34] because they generally involve post-synthetic methods. In order to circumvent these problems, we present a pre-synthetic strategy for modifying the surface properties of **MUV-1-Cl** with retention of the physical properties (magnetism). As a proof of concept, we have changed, by chemical design, the substituent in the fifth position (Cl in **MUV-1-Cl**) by different groups such as CH_3 (**MUV-1-CH_3**), H (**MUV-1-H**), Br (**MUV-1-Br**) and NH_2 (**MUV-1-NH_2**), thus tuning the behavior of the surface in contact with water from hydrophobicity values for contact angle to hydrophilicity (Figure 4). Alkane groups (H, CH_3) present values of contact angles of 99 ^{o} and 109 ^{o} respectively (i.e. moderate hydrophobic behavior); the inclusion of halides substituents causes an increase in the contact angle values (130^{o} and 135^{o} for Cl and Br, respectively), thus showing an increase in the hydrophobic character. On the contrary, the inclusion of the amino group (NH_2) causes a decrease of the contact angle value to 0 º, indicating superhydrophilic properties.

The five different ligands successfully employed already demonstrates large tunability, although we can anticipate that one of the possible limitations of this approach relies on the use of larger substituents that can interfere with the formation of the crystalline layered structure. However, preliminary results indicate that bulkier groups of up to 3 non-H atoms can also be incorporated with this approach, although further studies are still on-going.

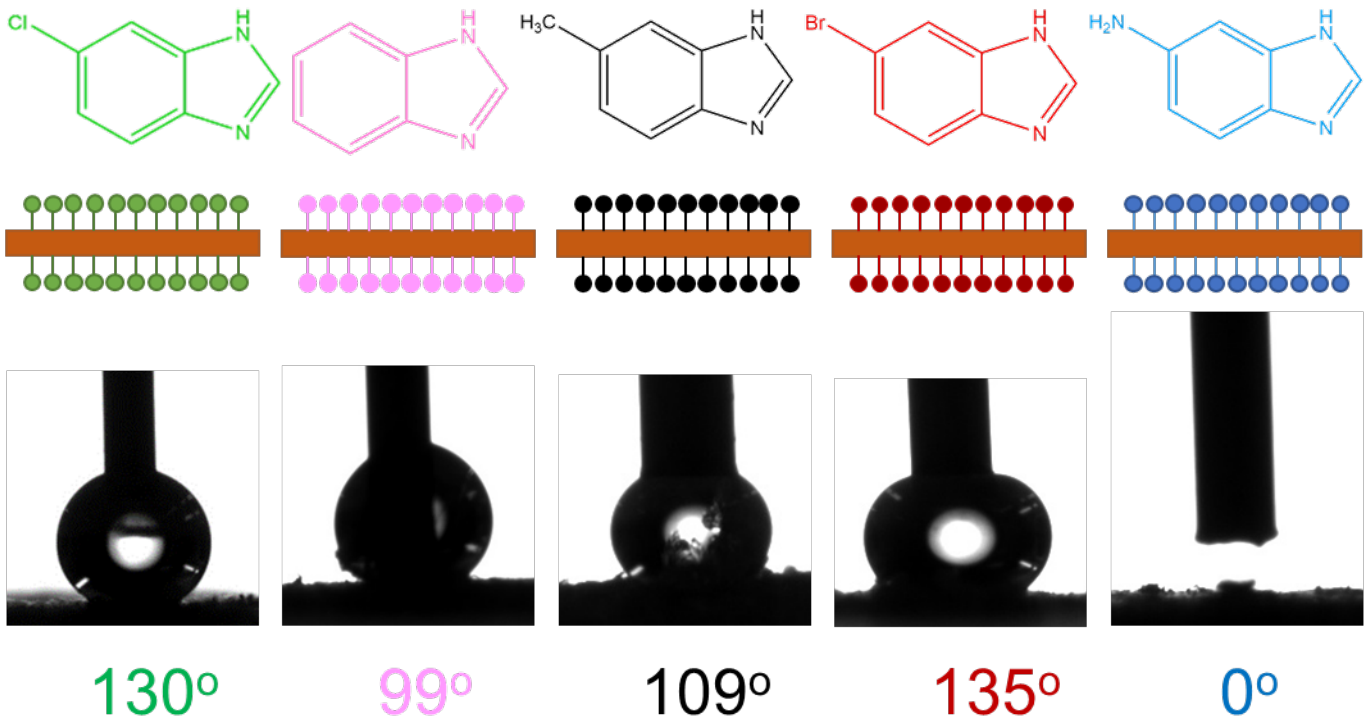

Figure 4 | Surface modification in MUV-1-X. The atoms at the surface of **MUV-1-X** can be changed by chemical design (X = Cl, H, CH_3, Br, NH_2) in a pre-synthetic manner in order to obtain different surface behaviors which change the water contact angle. No changes in the magnetic properties are observed upon the chemical modification (see Supporting Section 5).

The structural and magnetic properties of all these compounds have been characterized by X-ray diffraction, SQUID measurements, Mössbauer and Raman spectroscopies, SEM and TEM (Supplementary Information). Remarkably, the magnetic properties of the whole **MUV-1-X** family remains unaltered under the different surface modifications, as can be seen in Supplementary Table 4 and Supplementary Section 5.2. In addition, all the members from the **MUV-1-X** family have been exfoliated successfully by mechanically methods and characterized in detail as **MUV-1-Cl** (Supplementary Section 6).

The ability to tailor the functionality of **MUV-1-X**, combined with its mechanical resonant readout makes it attractive for sensing applications, because the resonance frequency and Q-factor of

these suspended membranes are expected to depend strongly on the mass and adhesion of captured molecules. To demonstrate this concept, we exfoliate and transfer thin flakes of **MUV-1-Cl** on top of a Si/SiO_2 substrate with prepatterned circular cavities. In Figure 5a we show optical images of two exemplary flakes transferred on top of cavities, forming suspended nanodrums. The AFM images of the drums (areas enclosed by the red boxes) are shown in Figure 5b. The device shown in the left panel of Figure 5a,b is 74 nm thick, whereas the thickness of the one shown in the right panel is measured to be 20 nm. In Figure 5c,d we show the mechanical frequency response of two **MUV-1-Cl** nanodrums (with thicknesses of 70 – 80 nm). The measurements are performed in vacuum, using a laser interferometry setup, described in the Methods section. The resonance frequencies of the drums are 38 MHz and 30.3 MHz, with quality (Q) factors in the range of 45 – 65. This variation may result from a combination of different thicknesses and geometries of the drums. The Q factors are comparable to those reported in nanomechanical resonators made of graphene and other two-dimensional materials.[35,36] The lower Q factors may be due to viscoelastic damping in this polymer material. Because of the large diameter-to-thickness ratio, the resonance frequencies of these nanodrums are mainly determined by the bending rigidity of the material. For the given resonance frequencies and geometry of the drums, we thus estimate the Young's modulus of **MUV-1-Cl** to be 3 – 7 GPa, which is almost three orders of magnitude lower than that of graphene and similar to that previously reported for a layered coordination polymer measured by AFM nanoindentation.[37] The results show that these polymer resonators, despite their low Young's modulus and despite potential viscous damping mechanisms, have surprisingly high Q factors and resonance frequencies, which are comparable to graphene membranes. In combination with their low weight and tunable functionalization these materials can be used to create future platforms for resonance based sensing.

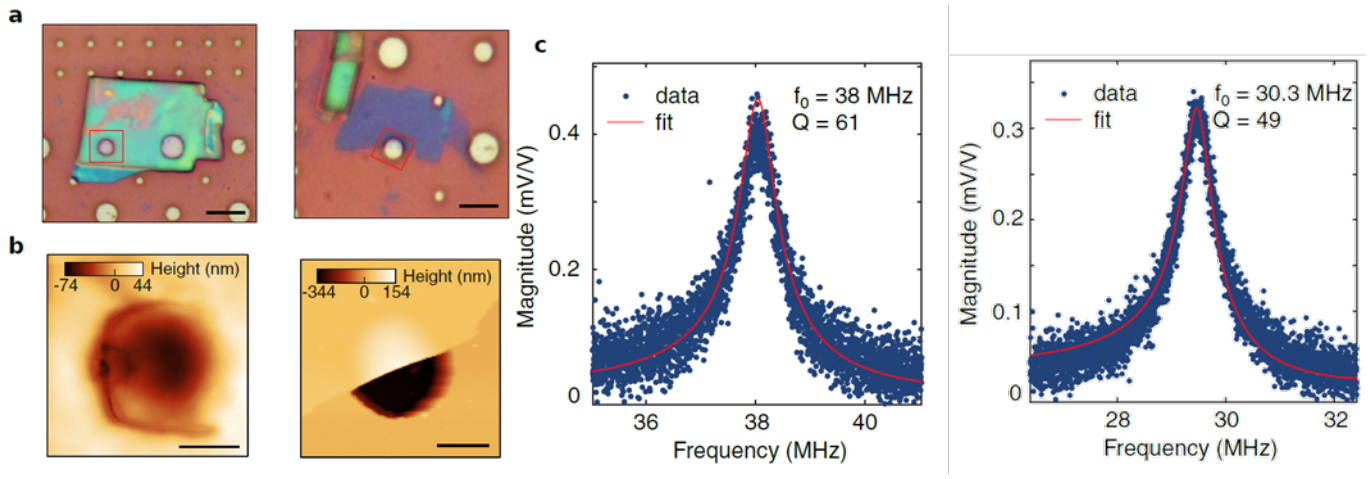

Figure 5 | MUV-1-Cl suspended membranes. a Optical images of two **MUV-1-Cl** flakes transferred on top of circular cavities on a Si/SiO_2 substrate (scale bars: 5 μm). left, the flake is 74 nm height; right, the flake is 20 nm height. The red boxes indicate the regions where AFM has been measured. **b** AFM images of the two drums taken in the area enclosed by the red boxes in **a** (scale bars: 1 μm). left, the drum corresponds to the flake of 74 nm height shown in panel a, left; right, the drum corresponds to the flake of 20 nm height shown in panel, a, right **c,** Two frequency-domain measurements on two different nanomechanical resonators made of **MUV-1-Cl**, with thicknesses of 70 – 80 nm. These are similar to the ones shown in panels **a,b**. The extracted resonance frequencies and quality factors of the two resonators are shown in the top right corner.

Discussion

In this work, we have presented a general strategy for the synthesis of crystalline layered coordination polymers (LCP) exhibiting a magnetic order and providing an unconventional route to tune at will the surface chemistry of the individual layers. In particular, by the election of different ligands, we have obtained a new family of LCP denoted as **MUV-1-X** (where X = Cl, Br, H, CH_3, or NH_2), with surface properties ranging from hydrophobic to hydrophilic, that retain their magnetic properties under the different surface modifications. Interestingly and in contrast with most of the reported MOFs, large crystals of these coordination polymers have been grown using a solvent-free synthesis. Such a possibility together with the layered nature of these materials and the very weak van der Waals forces between the layers have permitted isolation of micrometer size atomically-thin flakes down to the monolayer by

mechanical and dry exfoliation methods. The high crystallinity, integrity and chemical composition of these mechanically exfoliated layers has been confirmed by TEM and Raman studies on LCP of different thicknesses.

On the other hand, and in contrast to what happens in the few examples of reported 2D ferromagnets based on solid state chemistry,[13] which have shown to be highly unstable in open air, this coordination chemistry approach has afforded the isolation of robust 2D magnetic materials. Such a robustness has also enabled us to study the mechanical properties of these atomically-thin layers, a possibility that is unprecedented for coordination polymers. In fact, these 2D magnetic coordination polymers can lead towards the preparation of high quality resonators, a fundamental aspect in order to open up novel perspectives in the application of these materials in nanodevices. Thus, these results open the door to the integration and application of 2D coordination polymers in different technological areas like microfluidics, nanoelectronics, coatings, molecular sensing or mechanical magnetic membranes, and, last but not least, it brings new candidates for the study of magnetism and phase transitions in the two-dimensional limit. Finally, the variation of the wettability opens the possibility of creating complex stacked structures, where the interface can determine the formation of the heterostructure. Importantly, the pre-synthetic functionalization here described causes a perfect match with the periodicity of the 2D crystal, i.e. a perfect ligand decoration of the monolayer is obtained. This can permit the combination of this magnetic 2D material with superconductors or graphene, thus prompting to new materials where unconventional physical phenomena might be present, such as Majorana fermions or photomagnon couplings.

Methods

Synthesis of MUV-1-X. Ferrocene (30 mg, 0.16 mmol) and benzimidazole (or derivates) (0.34 mmol) were combined and sealed under vacuum in a layering tube (4 mm diameter). The mixture was heated at 250 °C for 3 days to obtain crystals suitable for X-ray single-crystal diffraction. The product was allowed

to cool to room temperature, and the layering tube was then opened. The unreacted precursors were extracted with acetonitrile and benzene, and the product was isolated as colorless crystals (yield 80 %). Phase purity was established by X-ray powder diffraction. Energy dispersive X-ray analysis (EDAX) of **MUV-1-Cl** from SEM and TEM show in both cases a 70:30 ratio for Cl:Fe.

X-ray Structural Studies. X-ray data for compounds **MUV-1-H** and **MUV-1-Cl** were collected at a temperature of 100 K using a synchrotron radiation at single crystal X-ray diffraction beamline I19 in Diamond Light Source, equipped with a Pilatus 2M detector and an Oxford Cryosystems nitrogen flow gas system. Data was measured using GDA suite of programs. X-ray data for compounds **MUV-1-Br**, **MUV-1-CH_3** and **MUV-1-NH_2** were collected at a temperature of 100/150 K using a Rigaku FR-X rotating anode diffractometer, equipped with Hybrid Photon detector HyPix-6000HE and an Oxford Cryosystems nitrogen flow gas system.

A summary of the data collection and structure refinements is provided in section 2 of the Supplementary Information.

AFM. Optical images were obtained with a NIKON Eclipse LV-100 Optical microscope and AFM images were performed with a Nanoscope IVa Multimode Scanning Probe Microscope (Bruker, Karlsruhe, Germany) in tapping mode.

TEM. Several mechanical exfoliated flakes were transferred onto a grid with a membrane of amorphous SiN (50 nm thick) using a dry and deterministic method (that involves the use of a micromanipulator and PDMS/PPC polymers, as reported in ref. [37]). TEM images and diffraction patterns were acquired with a JEOL JEM-2100F with a field emission gun operating at 200 kV. The simulated SAED patterns were generated with SingleCrystal software.

Contact Angle (CA) Measurements. Static water contact angle measurements of the samples were performed in air using a Rame-hart 200 standard goniometer equipped with an automated dispensing system. The initial drop volume was 0.17 μL, increased by additions of 0.08 μL.

MFM. Magnetic images were recorded with a commercial LT-MFM (attoMFM I, Attocube Systems AG) with a commercial magnetic-coated cantilever (Nanosensors PPP-MFMR). The sample was cooled down with an applied external out-of-plane field of +1 T, to assure that the tip magnetization was out-of-plane.

Magnetic Measurements. Variable-temperature (2−300 K) direct current (dc) magnetic susceptibility measurements were carried out in applied fields of 1.0 kOe and variable field magnetization measurements up to ± 5 T at 2.0 K. The susceptibility data were corrected from the diamagnetic contributions as deduced by using Pascal's constant tables. Variable-temperature (16−23 K) alternating current (ac) magnetic susceptibility measurements in a ±4.0 G oscillating field at frequencies in the range of 1 − 997 Hz were carried out in a zero dc field.

Nanomechanical resonators. Suspended membranes were fabricated by exfoliating **MUV-1-Cl** flakes directly on top of circular cavities lithographically defined on a Si/SiO2 substrate (SiO_2 thickness: 285 nm).

Laser interferometry measurements. The motion of the **MUV-1-X** mechanical resonators was measured in vacuum, using a laser interferometry setup, similar to the one reported in ref. [35]. A modulated blue laser is used to sequentially heat up the membrane, bringing it into motion. A different, red laser is focused onto the suspended membrane and is partly reflected by the membrane and partly by the silicon chip underneath. As the membrane moves, the effective cavity depth is modulated. This modulates the intensity of the reflected laser beam by interference, which is captured by a photodiode. The measurements were done in a homodyne detection scheme, using a vector network analyser.

All data generated and analysed during this study are included in this Article and its Supplementary Information, and are also available from the authors upon reasonable request. Atomic coordinates and structure factors for the reported crystal structures have been deposited in the Cambridge Crystallographic Data Centre (CCDC 1582347-1582350).

References

1. Ferrari, A. C. *et al.* Science and technology roadmap for graphene, related two-dimensional crystals, and hybrid systems. *Nanoscale* **7,** 4598–4810 (2015).

2. Dean, C. R. *et al.* Boron nitride substrates for high-quality graphene electronics. *Nat. Nanotechnol.* **5,** 722–726 (2010).

3. Mañas-Valero, S., García-López, V., Cantarero, A. & Galbiati, M. Raman spectra of ZrS_2 and $ZrSe_2$ from bulk to atomically thin layers. *Appl. Sci.* **6,** 264 (2016).

4. Mak, K. F., Lee, C., Hone, J., Shan, J. & Heinz, T. F. Atomically thin MoS_2: a new direct-gap semiconductor. *Phys. Rev. Lett.* **105,** 136805 (2010).

5. Carvalho, A. *et al.* Phosphorene: from theory to applications. *Nat. Rev. Mater.* **1,** 16061 (2016).

6. Acerce, M., Voiry, D. & Chhowalla, M. Metallic 1T phase MoS_2 nanosheets as supercapacitor electrode materials. *Nat. Nanotechnol.* **10,** 313–318 (2015).

7. Xu, C. *et al.* Large-area high-quality 2D ultrathin Mo_2C superconducting crystals. *Nat. Mater.* **14,** 1135–1141 (2015).

8. El-Bana, M. S. *et al.* Superconductivity in two-dimensional $NbSe_2$ field effect transistors. *Supercond. Sci. Technol.* **26,** 125020 (2013).

9. Navarro-Moratalla, E. *et al.* Enhanced superconductivity in atomically thin TaS_2. *Nat. Commun.* **7,** 11043 (2016).

10. Hardy, W. J. *et al.* Thickness-dependent and magnetic-field-driven suppression of antiferromagnetic order in thin V_5S_8 single crystals. *ACS Nano* **10,** 5941–5946 (2016).

11. Lee, J.-U. *et al.* Ising-type magnetic ordering in atomically thin $FePS_3$. *Nano Lett.* **16,** 7433–7438 (2016).

12. Gong, C. *et al.* Discovery of intrinsic ferromagnetism in two-dimensional van der Waals crystals. *Nature* **546,** 265–269 (2017).

13. Huang, B. *et al.* Layer-dependent ferromagnetism in a van der Waals crystal down to the monolayer limit. *Nature* **546,** 270–273 (2017).

14. Diercks, C. S. & Yaghi, O. M. The atom, the molecule, and the covalent organic framework. *Science.* **355,** 1585 (2017).

15. Liu, W. *et al.* A two-dimensional conjugated aromatic polymer via C–C coupling reaction. *Nat. Chem.* **9,** 563–570 (2017).

16. Rodríguez-San-Miguel, D., Amo-Ochoa, P. & Zamora, F. MasterChem: cooking 2D-polymers. *Chem. Commun.* **52,** 4113–27 (2016).

17. Peng, Y. *et al.* Metal-organic framework nanosheets as building blocks for molecular sieving membranes. *Science* **346,** 1356–1359 (2014).

18. Rodenas, T. *et al.* Metal–organic framework nanosheets in polymer composite materials for gas separation. *Nat. Mater.* **14,** 48–55 (2015).

19. Lahiri, N., Lotfizadeh, N., Tsuchikawa, R., Deshpande, V. V & Louie, J. Hexaaminobenzene as a building block for a family of 2D coordination polymers. *J. Am. Chem. Soc.* **139,** 19–22 (2017).

20. Araki, T., Kondo, A. & Maeda, K. The first lanthanide organophosphonate nanosheet by exfoliation of layered compounds. *Chem. Commun.* **49,** 552–554 (2013).

21. Abhervé, A., Mañas-Valero, S., Clemente-León, M. & Coronado, E. Graphene related magnetic materials: micromechanical exfoliation of 2D layered magnets based on bimetallic anilate complexes with inserted $[Fe^{III}(acac_2\text{-trien})]^+$ and $[Fe^{III}(sal_2\text{-trien})]^+$ molecules. *Chem. Sci.* **6,** 4665–4673 (2015).

22. Foster, J. A., Henke, S., Schneemann, A., Fischer, R. A. & Cheetham, A. K. Liquid exfoliation of alkyl-ether functionalised layered metal–organic frameworks to nanosheets. *Chem. Commun.* **52,** 10474–10477 (2016).

23. Shi, W. *et al.* Surface modification of two-dimensional metal–organic layers creates biomimetic catalytic microenvironments for selective oxidation. *Angew. Chem. Int. Ed.* **56,** 9704–9709 (2017).

24. Peng, Y. *et al.* Two-dimensional metal–organic framework nanosheets for membrane-based gas separation. *Angew. Chem. Int. Ed.* **56,** 9757–9761 (2017).

25. Lei, S. *et al.* Surface functionalization of two-dimensional metal chalcogenides by Lewis acid-base chemistry. *Nat. Nanotechnol.* **11,** 465–471 (2016).

26. Gaur, A. P. S. *et al.* Surface energy engineering for tunable wettability through controlled synthesis of MoS_2. *Nano Lett.* **14,** 4314–4321 (2014).

27. Faghani, A. *et al.* Controlled covalent functionalization of thermally reduced graphene oxide to generate defined bifunctional 2D nanomaterials. *Angew. Chem. Int. Ed.* **56,** 2675–2679 (2017).

28. Rettig, S. J., Storr, A., Summers, D. A., Thompson, R. C. & Trotter, J. Transition metal azolates from metallocenes. 2. Synthesis, X-ray structure, and magnetic properties of a three-dimensional polymetallic Iron(II) imidazolate complex, a low-temperature weak ferromagnet. *J. Am. Chem. Soc.* **119,** 8675–8680 (1997).

29. Lines, M. E. The quadratic-layer antiferromagnet. *J. Phys. Chem. Solids* **31,** 101–116 (1970).

30. Nguyen, L. *et al.* Atomic defects and doping of monolayer $NbSe_2$. *ACS Nano* **11,** 2894–2904 (2017).

31. Rooney, A. P. *et al.* Observing imperfection in atomic interfaces for van der Waals heterostructures. *Nano Lett.* **17,** 5222–5228 (2017).

32. Hartmann, U. Magnetic force microscopy. *Annu. Rev. Mater. Sci.* **29,** 53–87 (1999).

33. Serri, M. *et al.* Low-temperature magnetic force microscopy on single molecule magnet-based microarrays. *Nano Lett.* **17,** 1899–1905 (2017).

34. Zhu, X. *et al.* Signature of coexistence of superconductivity and ferromagnetism in two-dimensional $NbSe_2$ triggered by surface molecular adsorption. *Nat. Commun.* **7,** 11210 (2016).

35. Bunch, J. S. *et al.* Electromechanical resonators from graphene sheets. *Science* **315,** 490–493 (2007).

36. Castellanos-Gomez, A. *et al.* Single-layer MoS_2 mechanical resonators. *Adv. Mater.* **25,** 6719–6723 (2013).

37. Hermosa, C. *et al.* Mechanical and optical properties of ultralarge flakes of a metal–organic framework with molecular thickness. *Chem. Sci.* **6,** 2553–2558 (2015).

38. Britnell, L. *et al.* Strong light-matter interactions in heterostructures of atomically thin films. *Science* **340,** 1311–1314 (2013).

Acknowledgements

Financial support from the European Comission (COST Action MOLSPIN CA15128, FET-OPEN 2D-INK 664878, ERC-2016-CoG 724681-S-CAGE and ERC-2018-AdG 788222 Mol-2D), the Spanish MINECO (Structures of Excellence María de Maeztu MDM-2015-0538 and Severo Ochoa SEV-2012-0267, projects CTQ2014-59209-P, CTQ2017-89528-P, MAT2017-89993-R, MAT2015-68200-C2-2-P and MAT2015-71842-P), the Generalitat Valenciana (Prometeo programme), and the VLC/Campus Program is gratefully acknowledged. G.M.E. thanks the Spanish MINECO for a Ramón y Cajal Fellowship. S.M.V thanks MINECO for a predoctoral FPU grant (FPU14/04407). J.L.C. acknowledges the University of Valencia for an "Atracció de Talent" grant. C^2TN/IST authors acknowledge the

Portuguese Foundation for Science and Technology (FCT), contract UID/Multi/04349/2013. D.D., P.G.S and H.S.J.vdZ acknowledge the support of the Netherlands Organisation for Scientific Research (NWO/OCW), as part of the Frontiers of Nanoscience (NanoFront) program and the European Union Seventh Framework Programme under grant agreement number 604391 Graphene Flagship. We are grateful to the Spanish CRG-D1B at Institut Laue-Langevin for the allocated beamtime (project CRG-2402).

Author contributions

J.L.C and S.M.V contributed equally to this work; J.L.C. synthetized and characterized all the materials in bulk.; S.M.V. analyzed the magnetic data and did the MFM measurements; S.M.V. did the exfoliation and characterization of the exfoliated materials assisted by J.L.C.; I.J.V.Y. contributed to solution and refinement of the structures from single crystal data with the help of G.M.E.; P.J.B. conducted the TEM studies with contributions from J.L.C. and S.M.V.; J.A.R.V. performed the neutron diffraction studies; J.CW. and B.J.C.V. performed the Mossbauer characterization; D.D., P.G.S. and H.S.J.vdZ. characterized the nanomechanical resonators; G.M.E. and E.C. conceived and designed the experiments; J.LC., S.M.V., G.M.E and E.C. prepared the manuscript; all authors made comments on the manuscript.

Additional information

Supplementary Information is available in the online version of the paper. Correspondence and requests for materials should be addressed to G.M.E. or E.C.

Competing financial interests

The authors declare no competing financial interests.